Low-Energy Electron Diffraction*

Yiming Teng,† Xingyu Chen,‡ and Derap Pena Mukti Sari§
Université Paris-Saclay
(Dated: June 13, 2025)

We observed low-energy electron diffraction patterns on Cu(111) sample for two azimuthal angles and various energies. We find changing azimuthal angles only globally rotates the diffraction pattern, but an increase in the energy shrinks the pattern and results in a periodic hexagonal-triangle-hexagonal-opposite triangle pattern change. We argue that the shrinking of the pattern can be explained with the Bragg's law and geometric arguments, while the periodic pattern change can be understood by the heuristic picture where the Ewald's sphere intersects with reciprocal lattice points stretched perpendicularly due to finite-penetration-depth effect.

I. INTRODUCTION

In 1924, Louis de Broglie made a groundbreaking statement on the concept of matter-wave in his PhD thesis [1]. According to his analogy to the wave-matter duality of photons, matter particles like electrons also behave with waving properties. In particular, a matter particle with momentum $\boldsymbol{p}$ is associated with a de Broglie wavelength

$$\lambda \equiv \frac{h}{|\boldsymbol{p}|}, \tag{1}$$

where h is the Planck constant.

Denote the electron mass as m_e, if it is accelerated by an electric potential U, then according to the relativistic energy-momentum relation

$$\sqrt{p^2c^2 + m_e^2c^4} = eU + m_ec^2,$$

the electron wavelength should be

$$\lambda = \frac{h}{\sqrt{2m_eU + e^2U^2/c^2}} \approx \sqrt{\frac{1.5\ \mathrm{V}}{U}}\ \mathrm{nm}. \tag{2}$$

Therefore, if electrons do inherit wave properties, then a periodic structure with a characteristic scale at the order of $\sim$ nm should diffract electrons just like a grating diffracting light. Later, experiments conducted by C. J. Davisson, L. H. Germer, and G. P. Thomson *et. al.* confirmed the existence of electron diffraction, supporting de Broglie's theory while boosting the later development of quantum theory.

Electron diffraction has not only established its significance in the history of physics but has also been an important approach to studying atom distribution, crystallographic structure, and surface structure of the sample. Particularly, the small penetration depth (Figure 1) of low-energy electrons has made Low-Energy Electron Diffraction (LEED) particularly useful for surface analysis. In this experiment, we observed LEED patterns on Cu(111) sample for various acceleration voltages and azimuthal angles, highlighted differences and similarities between the patterns, and offered explanations for them based on diffraction theory.

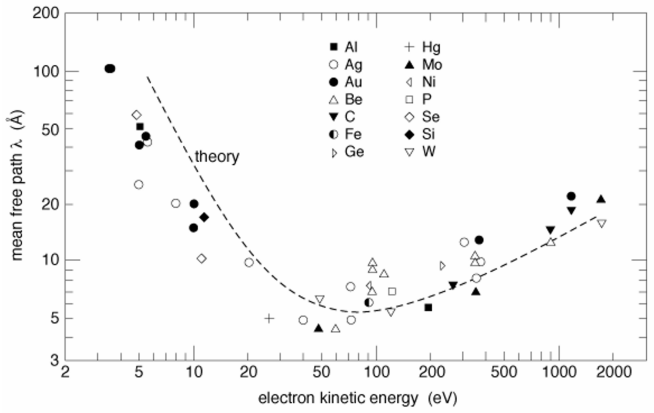

FIG. 1. Mean free path for electrons in various materials.

II. THEORETICAL FRAMEWORK

According to elementary quantum mechanics, the scattered out-state of a single electron in a potential $V(\boldsymbol{r})$ with plane-wave in-state $\psi_{\mathrm{in}}(\boldsymbol{r}) = \exp(\mathrm{i}\boldsymbol{k}_0 \cdot \boldsymbol{r})$ generally writes

$$\psi_{\mathrm{out}}(\boldsymbol{r}) = \psi_0(\boldsymbol{r}) + f(\boldsymbol{s})\frac{\exp(\mathrm{i}\boldsymbol{k} \cdot \boldsymbol{r})}{r}, \tag{3}$$

where $\boldsymbol{k}$ is the scattered wavevector detected, $\boldsymbol{s} \equiv \boldsymbol{k} - \boldsymbol{k}_0$ is the transferred wavevector during scattering. $f(\boldsymbol{s})$ is the so-called scattering amplitude, which only depends on details of the potential $V(\boldsymbol{r})$, and the first-order Born approximation shows

$$f(\boldsymbol{s}) = \frac{2\pi m_e e}{h^2}\int \mathrm{d}^3\boldsymbol{r}\ V(\boldsymbol{r})\exp(\mathrm{i}\boldsymbol{s} \cdot \boldsymbol{r}). \tag{4}$$

Denote the positions of atoms composing a basis in a crystal cell as $\boldsymbol{r}_i$, each of them contributes a potential $\varphi_i(\boldsymbol{r} - \boldsymbol{r}_i)$, then the total potential experienced by

---

* Lab Report at Université Paris-Saclay.
† yiming.teng@universite-paris-saclay.fr
‡ xingyu.chen@universite-paris-saclay.fr
§ derap-pena-mukti.sari@universite-paris-saclay.fr

the scattered electron writes (inter-atomic interactions ignored)

$$\phi_0(\boldsymbol{r}) = \sum_i \varphi_i(\boldsymbol{r} - \boldsymbol{r}_i). \tag{5}$$

Hence, the structure factor of the basis writes

$$\begin{aligned} F(\boldsymbol{s}) &= \frac{2\pi m_e e}{h^2} \int \mathrm{d}^3\boldsymbol{r} \left[\sum_i \varphi_i(\boldsymbol{r} - \boldsymbol{r}_i)\right] \exp(\mathrm{i}\boldsymbol{s}\cdot\boldsymbol{r}) \\ &= \frac{2\pi m_e e}{h^2} \sum_i \exp(2\pi\mathrm{i}\boldsymbol{s}\cdot\boldsymbol{r}_i) \int \mathrm{d}^3\mathbf{r}\ \varphi_i(\boldsymbol{r}) \exp(\mathrm{i}\boldsymbol{s}\cdot\boldsymbol{r}) \\ &\equiv \sum_i f_i(\boldsymbol{s}) \exp(\mathrm{i}\boldsymbol{s}\cdot\boldsymbol{r}_i), \end{aligned} \tag{6}$$

where f_i is the scattering amplitude of the i-th atom in the cell. Equation 6 exemplifies that, up to the level of the first-order Born approximation, the total scattering amplitude of a basis is a coherent superposition of single-atom scattering amplitudes of each atom in the cell.

A. Electron Diffraction by a Single-Crystal

Denote the three primitive vectors of a crystal Bravais lattice as $\boldsymbol{a}, \boldsymbol{b}, \boldsymbol{c}$, then the total potential of the single-crystal that the electron feels is

$$\begin{aligned} \phi(\boldsymbol{r}) &= \sum_{\ell,m,n} \phi_0(\boldsymbol{r} - \ell\boldsymbol{a} - m\boldsymbol{b} - n\boldsymbol{c}) \\ &= \int \mathrm{d}^3\boldsymbol{r}'\ \phi_0(\boldsymbol{r} - \boldsymbol{r}') \left[\sum_{\ell,m,n} \delta^3(\boldsymbol{r}' - \ell\boldsymbol{a} - m\boldsymbol{b} - n\boldsymbol{c})\right], \end{aligned} \tag{7}$$

where ϕ_0 is the total potential of the basis atoms in a crystal given in Equation 5. Hence the single-crystal scattering amplitude is

$$\begin{aligned} A(\boldsymbol{s}) &= \frac{2\pi m_e e}{h^2} \int \mathrm{d}^3\boldsymbol{r}\mathrm{d}^3\boldsymbol{r}'\ \varphi_0(\boldsymbol{r} - \boldsymbol{r}') \\ &\qquad \times \exp(\mathrm{i}\boldsymbol{s}\cdot\boldsymbol{r}) \left[\sum_{\ell,m,n} \delta^3(\boldsymbol{r}' - \ell\boldsymbol{a} - m\boldsymbol{b} - n\boldsymbol{c})\right] \\ &= F(\boldsymbol{s}) \int \mathrm{d}^3\boldsymbol{r}'\ \exp(\mathrm{i}\boldsymbol{s}\cdot\boldsymbol{r}') \\ &\qquad \times \left[\sum_{\ell,m,n} \delta^3(\boldsymbol{r}' - \ell\boldsymbol{a} - m\boldsymbol{b} - n\boldsymbol{c})\right] \\ &= F(\boldsymbol{s}) \sum_{\ell,m,n} \exp[\mathrm{i}\boldsymbol{s}\cdot(\ell\boldsymbol{a} + m\boldsymbol{b} + n\boldsymbol{c})]. \end{aligned} \tag{8}$$

Apparently, if $\boldsymbol{s}\cdot(\ell\boldsymbol{a} + m\boldsymbol{b} + n\boldsymbol{c}) \notin 2\pi\mathbb{Z}$, then the destructive interference of the complex phases in the summation will make modes with wavevector $\boldsymbol{s}$ only have zero scattering amplitudes. This motivates us to define the reciprocal vectors spanned by integer linear combinations of the basis vectors

$$\boldsymbol{a}^* = 2\pi \frac{\boldsymbol{b}\times\boldsymbol{c}}{\boldsymbol{a}\cdot(\boldsymbol{b}\times\boldsymbol{c})}, \tag{9}$$

$$\boldsymbol{b}^* = 2\pi \frac{\boldsymbol{c}\times\boldsymbol{a}}{\boldsymbol{a}\cdot(\boldsymbol{b}\times\boldsymbol{c})}, \tag{10}$$

$$\boldsymbol{c}^* = 2\pi \frac{\boldsymbol{a}\times\boldsymbol{b}}{\boldsymbol{a}\cdot(\boldsymbol{b}\times\boldsymbol{c})}, \tag{11}$$

whose integer linear combinations manifestly satisfy

$$(i\boldsymbol{a}^* + j\boldsymbol{b}^* + k\boldsymbol{c}^*)\cdot(\ell\boldsymbol{a} + m\boldsymbol{b} + n\boldsymbol{c}) \in 2\pi\mathbb{Z}. \tag{12}$$

Equation 8 now writes

$$\begin{aligned} A(\boldsymbol{s}) &= F(\boldsymbol{s}) \sum_{i,j,k} \delta^3(\boldsymbol{s} - i\boldsymbol{a}^* - j\boldsymbol{b}^* - k\boldsymbol{c}^*) \\ &= \sum_{i,j,k} F_{ijk}\delta^3(\boldsymbol{s} - i\boldsymbol{a}^* - j\boldsymbol{b}^* - k\boldsymbol{c}^*), \end{aligned} \tag{13}$$

where we have defined

$$F_{ijk} \equiv F(i\boldsymbol{a}^* + j\boldsymbol{b}^* + k\boldsymbol{c}^*). \tag{14}$$

We thus arrived at the Laue equation determining the position of diffraction patterns in single-crystal diffraction:

$$\boldsymbol{s} = \boldsymbol{k} - \boldsymbol{k}_0 = i\boldsymbol{a}^* + j\boldsymbol{b}^* + k\boldsymbol{c}^*. \tag{15}$$

The intensity of the pattern (ijk), denoted as I_{ijk}, should be proportional to the modulus square of the scattering amplitude F_{ijk}, therefore

$$\begin{aligned} I_{ijk} &\propto |F_{ijk}|^2 \\ &= \sum_{m,n} f_m(i\boldsymbol{a}^* + j\boldsymbol{b}^* + k\boldsymbol{c}^*)\bar{f}_n(i\boldsymbol{a}^* + j\boldsymbol{b}^* + k\boldsymbol{c}^*) \\ &\qquad \times e^{\mathrm{i}(i\boldsymbol{a}^* + j\boldsymbol{b}^* + k\boldsymbol{c}^*)\cdot(\boldsymbol{r}_m - \boldsymbol{r}_n)}. \end{aligned} \tag{16}$$

This implies that some special crystallographic structure could result in the disappearance of certain diffraction patterns.

B. Bragg's Law and Ewald's Sphere

We almost always assume elastic scattering in usual electron diffraction experiments; thus, the modulus of the out-going wavevector is the same as the in-coming wavevector. Denote the angle between $\boldsymbol{k}_0$ and $\boldsymbol{k}_{ijk}$ as $2\theta_{ijk}$, then we recover Bragg's law:

$$2|\boldsymbol{k}_0|\sin\theta_{ijk} = |i\boldsymbol{a}^* + j\boldsymbol{b}^* + k\boldsymbol{c}^*|. \tag{17}$$

Possible values for the out-going wavevectors shall correspond to the intersection of the reciprocal lattice and a sphere centered at the origin of the reciprocal lattice with radius $|\boldsymbol{k}_0|$ along the direction of $\boldsymbol{k}_0$, whose construction is shown in Figure 2. Obviously, the observed diffraction

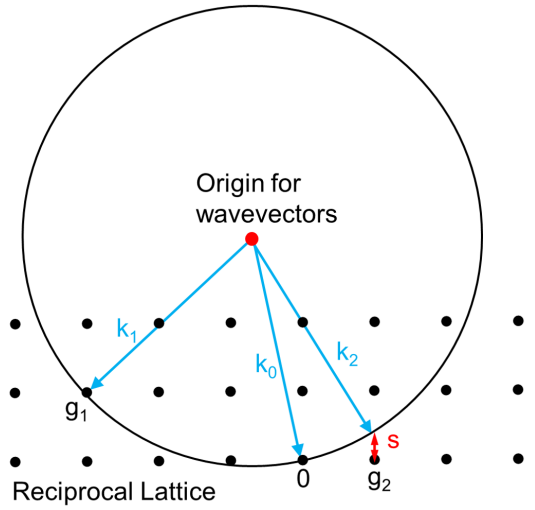

FIG. 2. Illustration of the Ewald's sphere [2].

pattern on a plane perpendicular to the direction of the incoming wavevector $\boldsymbol{k}_0$ is just the projection of the reciprocal lattice points intersected by Ewald's sphere onto this plane.

It's worth mentioning that although the penetration depth of electrons in materials is tiny, a few layers of atoms below the surface layer could still influence the diffraction. But their effect only manifests as "stretching" each reciprocal point in Figure 2 along the vertical direction into "reciprocal bars" [3], so certain diffraction patterns can be observed even if the Ewald's sphere doesn't precisely intersect their corresponding reciprocal lattice point. However, the pattern's intensity should be the strongest when the reciprocal lattice is exactly intersected.

C. Cu(111) Sample

The diffracted sample in this experiment is Cu(111) single-crystal. Copper usually has a face-centered cubic (fcc) structure, and the Cu(111) single-crystal sample is prepared so that its surface is aligned with the (111) crystal plane. Cooper atoms manifest a hexagonal arrangement on each (111) plane as illustrated on the left-hand side in Figure 3.

Ignoring the finite-penetration-depth effect discussed above, the electrons are only diffracted by the outmost layer, which can be regarded as a 2-dimensional hexagonal lattice. The corresponding reciprocal lattice is drawn on the right-hand side in Figure 3, and the first Brillouin zone is shaded. Following the convention in crystallography, high-symmetry points where the associated groups of the wave vector are non-trivial are labeled. For this two-dimensional case, the Miller indices labeling diffraction patterns becomes tuples $[ij]$, and the Bragg's law is reduced to

$$2|\boldsymbol{k}_0| \sin\theta_{ij} = |i\boldsymbol{a}^* + j\boldsymbol{b}^*|. \tag{18}$$

III. EXPERIMENTAL APPARATUS

The apparatus at the Tempo beamline in Soleil consists of three major parts, as shown in Figure 4:

- An electron gun to generate incident electron beams in the range energy with a variable acceleration voltage between 20 $\sim$ 500 V. The core of the electron gun unit is a filament. When heated, it releases free electrons. These electrons then pass through a Wehnelt cylinder (denoted as W) to achieve the initial collimation; after that, there are four electrostatic lenses to focus the electron beam on the sample and accelerate electrons at the same time.
- A goniometer to hold and orient the sample with precise measurements on angels. In particular, we rely on this device to achieve azimuthal rotations on the sample.
- A fluorescent screen monitoring diffracted patterns. Diffracted electrons hit this screen and result in visible fluorescent patterns. A camera is used to monitor and record the patterns.

All parts are enclosed in an ultra-high-vacuum chamber capable of reaching and maintaining pressures as low as $10^{-10} \sim 10^{-11}$ Torr to avoid electrons scattering with gas molecules.

IV. ANALYSIS

We varied the acceleration voltage to diffract electrons with various energies E for two different azimuthal angles, and the obtained diffraction patterns are shown in Figure 6 and Figure 7. In Figure 6, the azimuthal angle is set so that the horizontal direction is parallel to the $\Gamma - M$ direction in the reciprocal space, while in Figure 7, the azimuthal angle is rotated to ensure the horizontal direction is aligned with the $\Gamma - K$ direction. Obviously, the diffraction patterns from these two cases differ by a 30° rotation.

Both sets of diffraction patterns share two same features:

1. As the energy increases, the size of the diffraction pattern shrinks.
2. Diffraction patterns usually manifest a hexagonal structure, which is the same as the reciprocal lattice. However, for some energies, two sets of bright spots forming two interlocking regular triangles behave with different luminosities, or even one of the two sets is invisible.

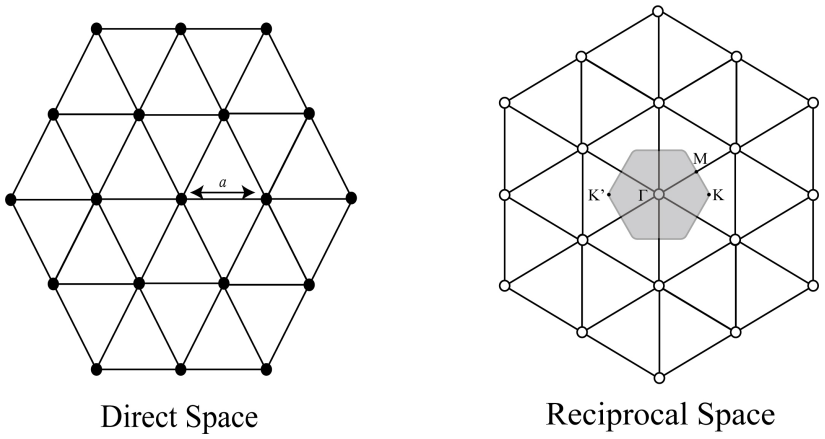

FIG. 3. Direct space and reciprocal space structures of the surface of the Cu(111) sample. High-symmetry points in the shaded first Brillouin zone are highlighted.

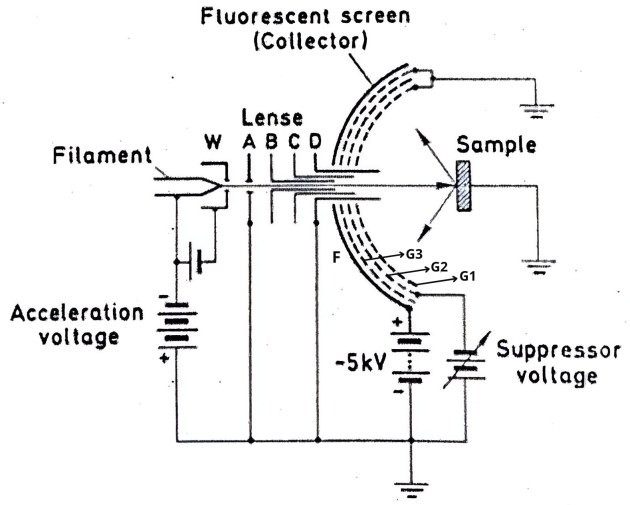

FIG. 4. Schematic illustration of the LEED experiments apparatus.

To understand the first feature, we focus on the diffraction pattern with Miller index $[ij]$ and assume its distance from the center of the diffraction pattern on the screen is R_{ij}. Denote the distance from the sample to the fluorescent screen as L_0 and assuming $L_0 \gg R_{ij}$ so that the diffraction angle $2\theta_{ij}$ is small, we would expect

$$2\theta_{ij} \approx \frac{R_{ij}}{L_0}. \tag{19}$$

Meanwhile, in small-angle approximation, the Bragg's law Equation 18 reduces to

$$2|\boldsymbol{k}_0|\theta_{ij} = |i\boldsymbol{a}^* + j\boldsymbol{b}^*|, \tag{20}$$

therefore

$$R_{ij} = \frac{|i\boldsymbol{a}^* + j\boldsymbol{b}^*|L_0}{|\boldsymbol{k}_0|} = \frac{|i\boldsymbol{a}^* + j\boldsymbol{b}^*|L_0}{2\pi}\lambda. \tag{21}$$

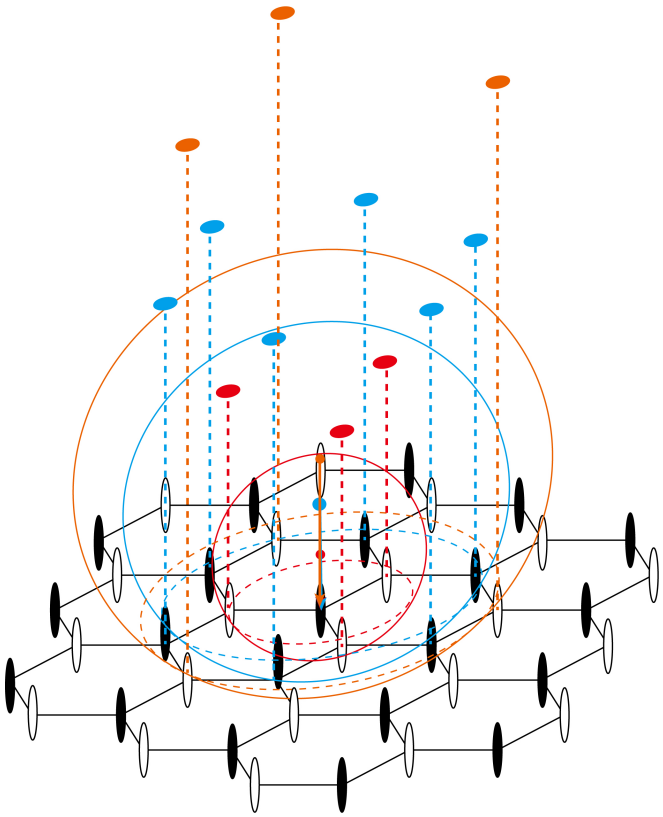

FIG. 5. Illustration of the intersection between the Ewald's sphere and the stretched reciprocal ellipsoids for different energies. To manifest the periodic change in the patterns, we demonstrated the hexagonal reciprocal lattice as two interlocking triangular lattices whose lattice points (ellipsoids) are respectively filled with black and white.

According to Equation 2, the wavelength λ scales as $U^{-1/2}$ with the acceleration voltage, therefore, R_{ij} also scales as $U^{-1/2}$ and the radii of the patterns indeed decrease as U increases.

The second feature can be explained with the Ewald's sphere and the finite-penetration-depth effect mentioned in II B. In the experiment, the actual effective reciprocal space doesn't contain point-like reciprocal points but consists "reciprocal ellipsoids" stretched along the direction perpendicular to the plane. As illustrated in Figure 5, varying the acceleration voltage amounts to change the radius of the Ewald's sphere, hence the positions where the sphere intersects with those reciprocal ellipsoids change, resulting in the luminosity change in the diffraction patterns. Sometimes, the sphere loses intersections with three ellipsoids arranged in a regualr triangular shape but establishes intersections with another three ellipsoids arranged also in a regular triangular shape but pointing at the opposite direction, hence we observe a periodic hexagonal-triangle-hexagonal-opposite triangle pattern change as we increase the acceleration voltage.

V. CONCLUSION

We observed low-energy electron diffraction patterns on Cu(111) sample. Diffraction patterns for two azimuthal angles and various acceleration voltages are recorded, they almost faithfully represent the features of the two-dimensional reciprocal lattice associated with the sample's surface atomic structure.In particular, we find the shrinking of the pattern size as the energy increases can be explained with the Bragg's law and some elementray geometric reasoning, and the periodic hexagonal-triangle-hexagonal-opposite triangle pattern change as we increase the acceleration voltage can be explained by the intersection between the Ewald's sphere and reciprocal lattice points stretched by finite-penetration-depth effect.

[1] L. de Broglie. Recherches sur la théorie des quanta. *Ann. de Phys*, 1924.

[2] Wikimedia Commons. File:ewald3.png — wikimedia commons, the free media repository, 2023. [Online; accessed 17-December-2024].

[3] Kun Xun Sicheng Wu. *Modern Physics Experiments*. Higher Education Press, 4 edition, 2015.

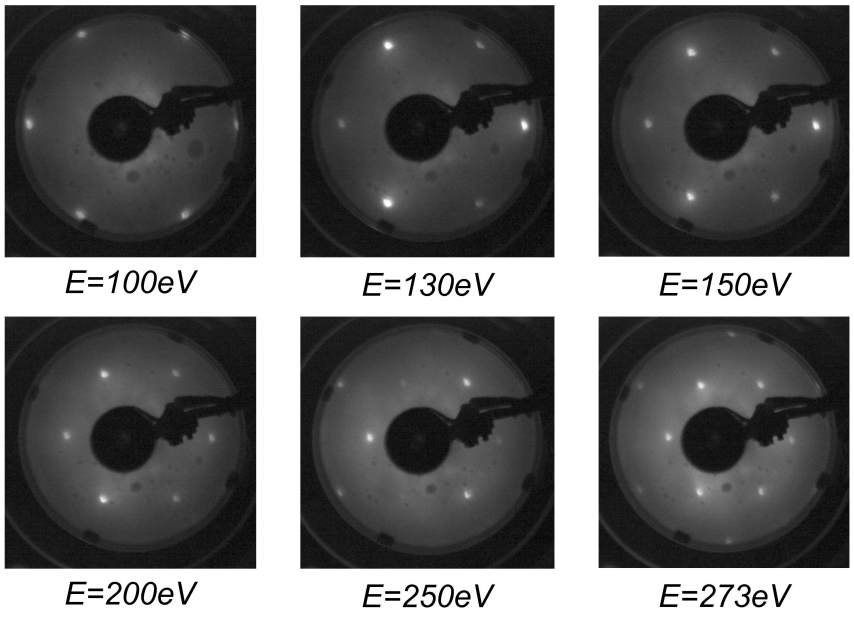

FIG. 6. Diffraction patterns. The azimuthal angle is set so that the horizontal direction is parallel to the $\Gamma - M$ direction.

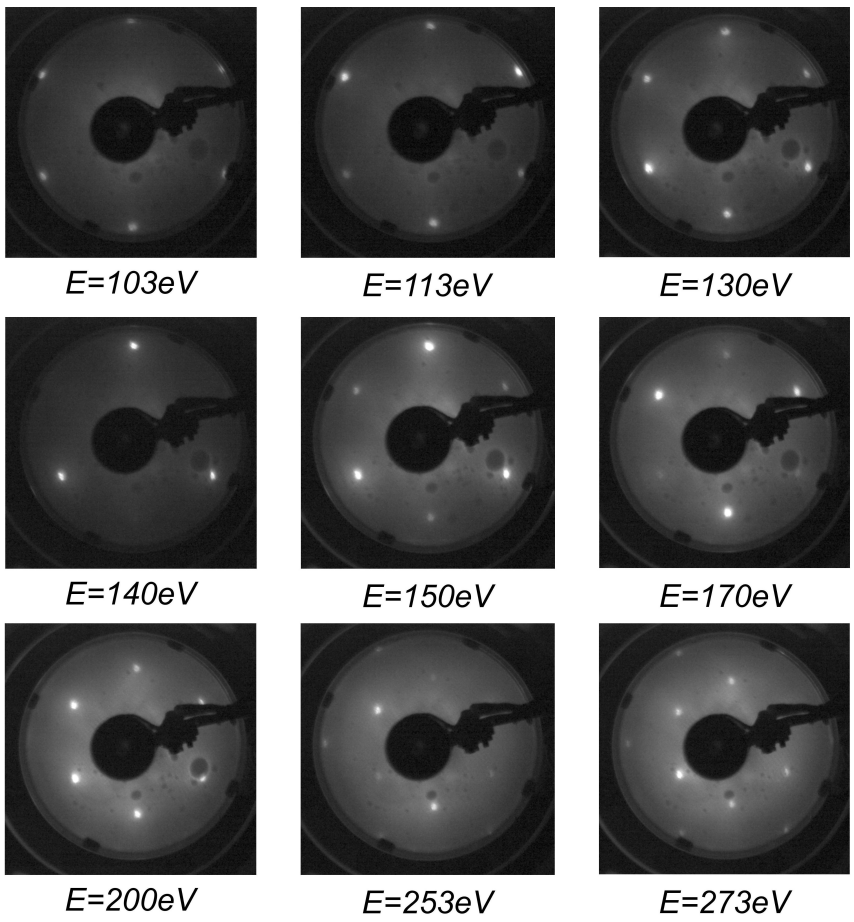

FIG. 7. Diffraction patterns. The azimuthal angle is rotated so that the horizontal direction is parallel to the $\Gamma - K$ direction.